Analysis of Gimbal Lock in Euler-Based Drone Orientation and Its Mitigation Using Quaternions

Agatha Tatianingseto - 13524008[1,2]
Program Studi Teknik Informatika
Sekolah Teknik Elektro dan Informatika
Institut Teknologi Bandung, Jl. Ganesha 10 Bandung 40132, Indonesia
[1]13524008@mahasiswa.itb.ac.id, [2]atia.seto@gmail.com

***Abstract*—Gimbal lock is a singularity in Euler-angle parameterizations of 3D rotation that can cause loss of one degree of freedom and severe coupling between yaw and roll near pitch $\pm 90^\circ$. This paper analyzes how the singularity appears in Euler-based drone orientation updates and demonstrates mitigation using unit quaternions, which provide a globally nonsingular attitude representation. Presented three experiments: (i) a static ambiguity test at the gimbal-lock pose, (ii) a dynamic propagation comparison under a maneuver that approaches the singular configuration, and (iii) a control-mixing test under a pure yaw command near pitch 90°. The results show that Euler representations become non-unique and ill-conditioned near the singularity, while quaternion propagation remains smooth and numerically stable.**

Keywords– attitude representation, Euler angles, gimbal lock, quaternions, drone navigation

I. Introduction

Unmanned aerial vehicles (UAVs), commonly referred to as drones, rely heavily on accurate orientation (attitude) representation for navigation, stabilization, and control. Orientation information is fundamental to tasks such as maintaining flight stability, executing precise maneuvers, sensor fusion, and trajectory tracking. Any ambiguity or numerical instability in the representation of orientation can directly lead to degraded control performance, unexpected motion, or even loss of the vehicle. Consequently, the choice of attitude representation is a critical design decision in drone navigation and control systems.

Euler angles, typically expressed as roll, pitch, and yaw, are among the most commonly used orientation representations in aerial robotics. Their popularity stems from their intuitive geometric interpretation and their direct correspondence to physical rotations of an aircraft body around its principal axes. Euler angles are also easy to visualize, interpret, and interface with human operators, making them a natural choice for high-level control, visualization, and debugging. As a result, many introductory flight control systems and navigation frameworks adopt Euler angles as their primary representation [1].

Despite their intuitive appeal, Euler angles suffer from a fundamental limitation known as *gimbal lock*. Gimbal lock occurs when two of the three rotation axes become aligned, resulting in the loss of one degree of freedom in the representation. For commonly used yaw–pitch–roll (ZYX) conventions, this singularity arises when the pitch angle approaches $\pm 90^\circ$. At this configuration, the mapping between angular velocity and Euler angle rates becomes ill-conditioned, and distinct Euler angle parameter sets can represent the same physical orientation. In the context of drone navigation and control, this singularity can lead to numerical instability, ambiguous orientation updates, and unintended coupling between control axes, such as yaw and roll. These effects are particularly dangerous during aggressive maneuvers or near-vertical flight, where reliable attitude estimation and control are essential [2].

To overcome the limitations of Euler-angle-based representations, modern drone systems widely adopt quaternions for internal attitude representation. Quaternions provide a compact and continuous parameterization of three-dimensional rotations without singularities. By representing orientation as a unit quaternion in four-dimensional space, quaternion-based formulations avoid gimbal lock entirely and allow smooth and stable attitude propagation for all possible orientations. Although quaternions are less intuitive than Euler angles for human interpretation, they are well suited for numerical integration, sensor fusion, and feedback control, which explains their widespread use in flight controllers, inertial navigation systems, and robotics software frameworks [3].

This paper analyzes the manifestation of gimbal lock in Euler-based drone orientation and demonstrates how quaternion-based representations mitigate the associated singularities. Through a series of static, dynamic, and control-oriented experiments, it shows how Euler angles become non-unique and ill-conditioned near the gimbal-lock configuration, while quaternion-based propagation remains stable and consistent under identical conditions. The results highlight that gimbal lock is not a physical limitation of rotational motion, but rather a singularity arising from the mathematical representation of orientation.

II. Theory

A. Euler Angles and Euler-Based Orientation

Euler angles represent three-dimensional orientation using three sequential rotations about coordinate axes. In aerial robotics, these rotations are commonly referred to as *roll*, *pitch*, and *yaw*, which correspond to rotations about the body-fixed x-, y-, and z-axes, respectively. This representation is intuitive, as it directly reflects the physical motions of an aircraft.

In this work, adopted the widely used ZYX (yaw–pitch–roll) convention, where orientation is constructed by a rotation about the z-axis (yaw ψ), followed by a rotation about the y-axis (pitch θ), and finally a rotation about the x-axis (roll ϕ). The overall rotation matrix $R \in SO(3)$ is given by

$$R(\phi, \theta, \psi) = R_z(\psi)\, R_y(\theta)\, R_x(\phi), \tag{1}$$

where

$$R_x(\phi) = \begin{bmatrix} 1 & 0 & 0 \\ 0 & \cos\phi & -\sin\phi \\ 0 & \sin\phi & \cos\phi \end{bmatrix}, \tag{2}$$

$$R_y(\theta) = \begin{bmatrix} \cos\theta & 0 & \sin\theta \\ 0 & 1 & 0 \\ -\sin\theta & 0 & \cos\theta \end{bmatrix}, \tag{3}$$

$$R_z(\psi) = \begin{bmatrix} \cos\psi & -\sin\psi & 0 \\ \sin\psi & \cos\psi & 0 \\ 0 & 0 & 1 \end{bmatrix}. \tag{4}$$

Because Euler angles describe orientation through *sequential rotations*, the order of multiplication in (1) is critical. Changing the rotation order produces a different orientation, even when the same angle values are used. This order dependence reflects the non-commutative nature of three-dimensional rotations and is a fundamental characteristic of Euler-based representations [1].

B. Gimbal Lock as a Singular Representation

A *singular representation* is a parameterization that fails to uniquely or smoothly describe all valid physical configurations of a system. In the context of Euler angles, singularity arises when the mapping between Euler parameters and physical orientation loses rank, resulting in the loss of one rotational degree of freedom [4].

For the ZYX convention, gimbal lock occurs when the pitch angle satisfies

$$\cos\theta = 0 \quad \Longleftrightarrow \quad \theta = \pm 90^\circ. \tag{5}$$

At this configuration, the first and third rotation axes become aligned, causing yaw and roll to become indistinguishable.

This singularity can be observed mathematically in the relationship between body angular velocity $\boldsymbol{\omega} = [\omega_x, \omega_y, \omega_z]^T$ and Euler angle rates $[\dot{\phi}, \dot{\theta}, \dot{\psi}]^T$, which for the ZYX convention can be expressed as [5]

$$\begin{bmatrix} \dot{\phi} \\ \dot{\theta} \\ \dot{\psi} \end{bmatrix} = \begin{bmatrix} 1 & \sin\phi\tan\theta & \cos\phi\tan\theta \\ 0 & \cos\phi & -\sin\phi \\ 0 & \sin\phi\sec\theta & \cos\phi\sec\theta \end{bmatrix} \boldsymbol{\omega}. \tag{6}$$

As $\theta \to \pm 90^\circ$, the terms $\tan\theta$ and $\sec\theta$ grow unbounded, rendering the mapping in (6) ill-conditioned. Consequently, small angular velocities can produce arbitrarily large Euler angle rates, leading to numerical instability and ambiguous orientation updates.

Furthermore, at the gimbal-lock configuration, the Euler parameterization becomes non-unique: multiple combinations of yaw and roll angles correspond to the same physical orientation. This non-uniqueness directly reflects the loss of one degree of freedom and is a defining characteristic of gimbal lock [5].

C. Quaternion Representation of Orientation

Quaternions provide an alternative representation of three-dimensional rotations that avoids the singularities inherent in Euler angles [2]. A quaternion is defined as

$$q = q_0 + q_1\mathbf{i} + q_2\mathbf{j} + q_3\mathbf{k}, \tag{7}$$

or equivalently as a vector

$$q = [q_0,\, q_1,\, q_2,\, q_3]^T, \tag{8}$$

subject to the unit-norm constraint $\|q\| = 1$.

A unit quaternion represents a rotation of angle α about a unit axis $\mathbf{u} \in \mathbb{R}^3$ through the axis–angle relationship [2]

$$q = \begin{bmatrix} \cos(\alpha/2) \\ \mathbf{u}\sin(\alpha/2) \end{bmatrix}. \tag{9}$$

Quaternion-based orientation propagation is governed by the kinematic equation [3]

$$\dot{q} = \frac{1}{2}\,\Omega(\boldsymbol{\omega})\, q, \tag{10}$$

where

$$\Omega(\boldsymbol{\omega}) = \begin{bmatrix} 0 & -\omega_x & -\omega_y & -\omega_z \\ \omega_x & 0 & \omega_z & -\omega_y \\ \omega_y & -\omega_z & 0 & \omega_x \\ \omega_z & \omega_y & -\omega_x & 0 \end{bmatrix}. \tag{11}$$

Unlike the Euler-rate mapping in (6), the quaternion kinematics in (10) contains no singular terms and remains well-defined for all orientations. As a result, quaternion representations provide a globally nonsingular parameterization of $SO(3)$, enabling smooth and stable orientation propagation even at configurations where Euler angles experience gimbal lock [5].

III. Methodology

This section describes the methodology used to analyze gimbal lock in Euler-based orientation and to evaluate the effectiveness of quaternion-based mitigation. To ensure a fair and meaningful comparison, Euler-angle and quaternion representations are propagated in parallel under identical conditions, and their resulting orientations are evaluated using well-defined geometric metrics [5].

A. Orientation Propagation Framework

The core methodology of this study is based on two parallel orientation propagation pipelines: an Euler-angle-based pipeline and a quaternion-based pipeline. Both pipelines represent the same physical orientation of a rigid body and are driven by identical body angular velocity inputs, following established comparative frameworks in attitude representation analysis [5].

1) Euler-Based Orientation Propagation

In the Euler-based pipeline, orientation is represented by roll, pitch, and yaw angles (ϕ, θ, ψ) using the ZYX convention. Given the body angular velocity

$$\boldsymbol{\omega} = [\omega_x,\ \omega_y,\ \omega_z]^T, \tag{12}$$

the corresponding Euler angle rates are obtained via the Euler-rate mapping [2], [5]

$$\begin{bmatrix} \dot{\phi} \\ \dot{\theta} \\ \dot{\psi} \end{bmatrix} = \mathbf{T}(\phi, \theta)\boldsymbol{\omega}, \tag{13}$$

where $\mathbf{T}(\phi, \theta)$ is the ZYX transformation matrix containing $\tan\theta$ and $\sec\theta$ terms.

The Euler angles are propagated through numerical integration,

$$\boldsymbol{\eta}_{k+1} = \boldsymbol{\eta}_k + \dot{\boldsymbol{\eta}}_k \Delta t, \tag{14}$$

where $\boldsymbol{\eta} = [\phi, \theta, \psi]^T$ and Δt is the integration time step. The updated Euler angles are converted into a rotation matrix $R_e \in SO(3)$ for evaluation.

2) Quaternion-Based Orientation Propagation

In the quaternion-based pipeline, orientation is represented by a unit quaternion $q \in \mathbb{R}^4$. Quaternion kinematics are governed by [3]

$$\dot{q} = \frac{1}{2}\Omega(\boldsymbol{\omega})q, \tag{15}$$

where $\Omega(\boldsymbol{\omega})$ is the skew-symmetric quaternion matrix.

Discrete-time propagation is performed as

$$q_{k+1} = q_k \otimes \delta q_k, \tag{16}$$

where δq_k represents the incremental rotation derived from the angular velocity. Quaternion normalization is applied after each update to enforce $\|q\| = 1$ [2]. The propagated quaternion is then converted into a rotation matrix $R_q \in SO(3)$.

3) Fair Comparison Conditions

To ensure that any observed discrepancies arise solely from representational properties, both pipelines satisfy the following conditions:

- Identical initial physical orientation.
- Identical angular velocity input $\boldsymbol{\omega}(t)$.
- Identical numerical integration parameters.

This ensures that differences between R_e and R_q can be attributed directly to representational behavior rather than external factors [5].

B. Evaluation Metrics

To quantitatively assess the behavior of Euler-angle and quaternion-based orientation propagation, several complementary metrics are employed, capturing both geometric discrepancies and representation-specific artifacts [1].

1) Rotation Matrix Comparison

Both Euler-angle and quaternion representations are converted into rotation matrices $R_e, R_q \in SO(3)$, allowing orientation comparison independently of the underlying parameterization.

2) Orientation Error on $SO(3)$

The orientation error is computed using the geodesic distance on $SO(3)$ [6]

$$\theta_{\text{err}} = \cos^{-1}\left(\frac{\text{trace}(R_e^T R_q) - 1}{2}\right), \tag{17}$$

which represents the minimum rotation angle required to align the two orientations.

3) Forward Vector Deviation

Let $\mathbf{f} = [1, 0, 0]^T$ denote the forward body-axis vector. The propagated forward directions are given by

$$\mathbf{f}_e = R_e\mathbf{f}, \quad \mathbf{f}_q = R_q\mathbf{f}. \tag{18}$$

The angular deviation between these vectors is used to evaluate heading discrepancies [2].

4) Euler Parameter Error

Euler angles extracted from quaternion-based orientation are compared against directly propagated Euler angles. Differences in yaw and roll are analyzed to identify parameter coupling and drift effects near singular configurations [5].

5) Decision Criterion

Euler-angle propagation is considered to fail when it exhibits numerical instability, non-uniqueness, or significant divergence from quaternion-based orientation under identical conditions. Quaternion-based propagation is considered successful if it remains smooth and consistent across all tested configurations.

IV. Experimental Design

This section describes the experimental setups used to investigate the limitations of Euler-based orientation representations and to evaluate the behavior of quaternion-based propagation under identical conditions. Each experiment is designed to isolate a specific aspect of gimbal lock or its practical implications in drone orientation and control. At this stage, the experiments are introduced descriptively, without interpretation or analysis of results.

A. Experiment A: Static Ambiguity at the Gimbal-Lock Configuration

Experiment A is designed to examine the static behavior of Euler-angle representations at the gimbal-lock configuration. The pitch angle is fixed at

$$\theta = 90^\circ, \tag{19}$$

which satisfies the gimbal-lock condition for the ZYX convention [2].

With the pitch angle held constant, multiple combinations of yaw ψ and roll ϕ are constructed such that

$$(\phi,\, \theta,\, \psi) \quad \text{and} \quad (\phi + \Delta,\, \theta,\, \psi - \Delta) \tag{20}$$

are evaluated for varying values of Δ.

Each Euler-angle triplet is converted into a rotation matrix

$$R_e = R_z(\psi) R_y(\theta) R_x(\phi), \tag{21}$$

and the resulting matrices are compared to determine whether distinct Euler parameters correspond to identical physical orientations. Quaternion representations corresponding to the same physical rotations are also computed for reference [5].

B. Experiment B: Dynamic Orientation Propagation

Experiment B evaluates the behavior of Euler-angle and quaternion-based orientation propagation under continuous motion. Both representations are initialized to the same physical orientation and are propagated forward in time using identical angular velocity inputs.

Orientation evolution is computed through discrete-time integration over a fixed simulation horizon. For Euler angles, the propagation follows

$$\boldsymbol{\eta}_{k+1} = \boldsymbol{\eta}_k + \mathbf{T}(\phi_k, \theta_k)\boldsymbol{\omega}_k \Delta t, \tag{22}$$

where $\boldsymbol{\eta} = [\phi, \theta, \psi]^T$ and $\mathbf{T}(\cdot)$ is the Euler-rate mapping matrix [5].

In parallel, quaternion propagation is performed using

$$q_{k+1} = q_k \otimes \delta q_k, \tag{23}$$

where δq_k represents the incremental rotation derived from the angular velocity $\boldsymbol{\omega}_k$ over the time step Δt [3].

The angular velocity input is chosen such that the pitch angle gradually increases over time, driving the system toward the gimbal-lock configuration. At each time step, both representations are converted into rotation matrices for subsequent comparison.

C. Experiment C: Control Mixing Under Pure Yaw Command

Experiment C investigates the effect of gimbal lock on control-oriented commands. The system is initialized with a pitch angle close to the singular configuration,

$$\theta \approx 89^\circ, \tag{24}$$

while roll and yaw are initially set to zero.

A pure yaw angular velocity command is applied,

$$\boldsymbol{\omega} = \begin{bmatrix} 0 \\ 0 \\ \omega_z \end{bmatrix}, \tag{25}$$

with ω_z held constant throughout the simulation.

Euler-angle and quaternion-based propagations are again executed in parallel under identical numerical conditions. The resulting orientations are converted into rotation matrices and used to propagate the forward body-axis vector. Any deviation from a purely yaw-induced motion is recorded for subsequent analysis [2].

V. Gimbal Lock in Euler-Based Orientation

This section presents experimental evidence illustrating how gimbal lock manifests in Euler-based orientation representations. Using static and dynamic experiments, demonstrate the loss of uniqueness and numerical stability that occurs when Euler angles approach their singular configuration.

A. Non-Unique Euler Parameterization at Pitch = 90°

This subsection analyzes the static behavior of Euler-angle representations at the gimbal-lock configuration using Experiment A. The pitch angle is fixed at $\theta = 90^\circ$, while yaw and roll angles are varied according to two parameterizations:

$$(\phi, \theta, \psi) = (0, 90^\circ, \alpha), \tag{26}$$

and

$$(\phi, \theta, \psi) = (\alpha, 90^\circ, 0). \tag{27}$$

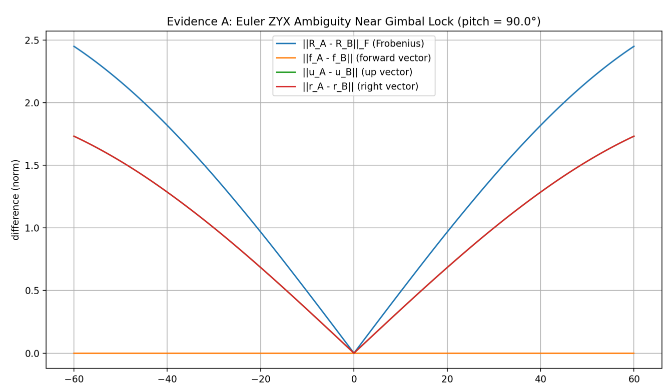

Fig. 1. Static ambiguity of Euler ZYX representation at $\theta = 90^\circ$, showing identical orientations for distinct yaw–roll parameterizations (Experiment A).

Despite having different Euler parameters, both configurations produce identical rotation matrices. Figure 1 shows that the Frobenius norm of the difference between the resulting rotation matrices is zero at $\alpha = 0$ and symmetric for positive and negative values of α, indicating that multiple Euler angle triples map to the same physical orientation.

This ambiguity arises because, at $\theta = 90°$, the first and third rotation axes become aligned. Consequently, yaw and roll rotations are no longer independent, and the Euler representation loses one degree of freedom. From a mathematical perspective, this corresponds to a rank deficiency in the Jacobian of the Euler-angle mapping, which directly characterizes gimbal lock.

Therefore, Experiment A demonstrates that gimbal lock is not a numerical artifact but a fundamental representational failure, where orientation can no longer be uniquely parameterized by Euler angles.

B. *Ill-Conditioned Orientation Propagation Near the Singular Pose*

Experiment B evaluates the dynamic consequences of gimbal lock by propagating orientation over time while the pitch angle approaches the singular configuration. Euler-angle and quaternion-based representations are propagated in parallel using identical angular velocity inputs.

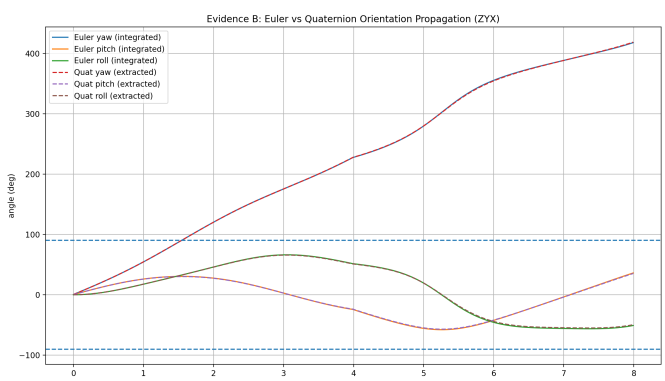

Fig. 2. Time evolution of Euler angles from direct Euler integration and quaternion-based propagation (Experiment B).

Figure 2 shows the time evolution of Euler angles obtained through direct Euler integration and those extracted from quaternion propagation. While both representations initially agree, noticeable divergence appears as the pitch angle approaches $\pm 90°$.

This divergence is explained by the Euler-rate mapping, which contains $\tan \theta$ and $\sec \theta$ terms. As $\theta \to \pm 90°$, these terms grow unbounded, causing small angular velocities to induce large Euler angle rates. Figure 3 confirms this behavior, showing a sharp increase in Euler rate magnitudes near the singular configuration.

The resulting orientation discrepancy is quantified using the $SO(3)$ geodesic distance. As shown in Figure 4, the orientation error between Euler-based and quaternion-based propagation increases monotonically over time, indicating cumulative divergence caused by ill-conditioned Euler dynamics.

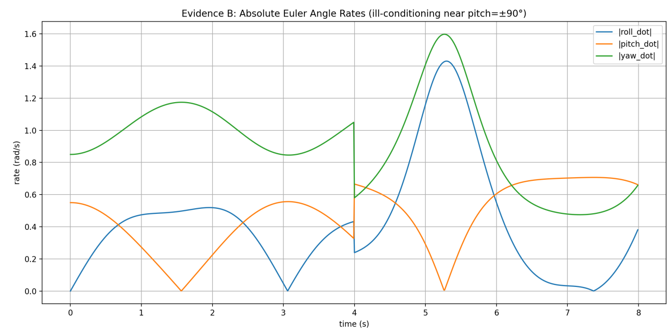

Fig. 3. Absolute Euler angle rates showing ill-conditioning as pitch approaches $\pm 90°$ (Experiment B).

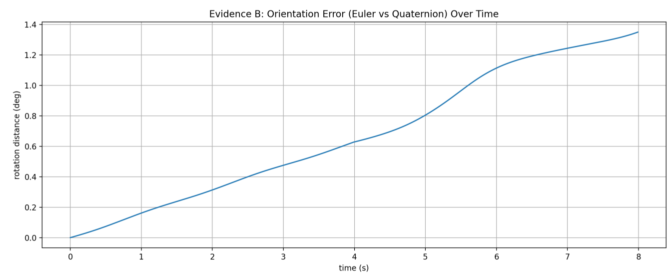

Fig. 4. Orientation error on $SO(3)$ between Euler-based and quaternion-based propagation over time (Experiment B).

These results demonstrate that gimbal lock significantly degrades time-based orientation updates, even when the system does not remain exactly at the singular pose.

VI. Quaternion-Based Mitigation of Euler Singularities

While Section V demonstrated the failure modes of Euler-based orientation representations, this section examines the same experimental results from the perspective of quaternion-based propagation. By directly comparing Euler and quaternion outcomes under identical conditions, we show that quaternions maintain stable, continuous, and physically consistent orientation behavior across configurations where Euler angles exhibit singularities.

A. *Smooth Orientation Propagation Through Singular Configurations*

The effectiveness of quaternion-based orientation propagation is evident in the results of Experiment B, which compares Euler-angle integration and quaternion propagation under increasing pitch motion.

Figure 2 shows the evolution of roll, pitch, and yaw angles obtained through direct Euler integration alongside Euler angles extracted from quaternion-based propagation. While both representations initially follow similar trajectories, discrepancies begin to emerge as the pitch angle approaches $\pm 90°$.

This divergence is further clarified in Fig. 3, which plots the absolute Euler angle rates over time. Near the gimbal-lock configuration, the Euler-based roll and yaw rates exhibit sharp peaks caused by the $\tan\theta$ and $\sec\theta$ terms in the Euler-rate mapping. In contrast, the quaternion-based orientation does not exhibit any corresponding instability, as its propagation is governed by a nonsingular kinematic equation.

The cumulative effect of these instabilities is quantified in Fig. 4, which shows the orientation error on $SO(3)$ between Euler-based and quaternion-based rotation matrices. The monotonic increase in orientation error demonstrates that Euler-based propagation progressively diverges from the physically consistent quaternion trajectory as the system approaches the singular configuration.

Together, these results show that quaternion-based propagation remains smooth and well-conditioned across all tested orientations, providing a stable reference even when Euler-based representations become unreliable.

B. Elimination of Control Mixing Under Pure Yaw Commands

Experiment C investigates the impact of orientation representation on control behavior by applying a pure yaw angular velocity command to a system initialized near the gimbal-lock configuration.

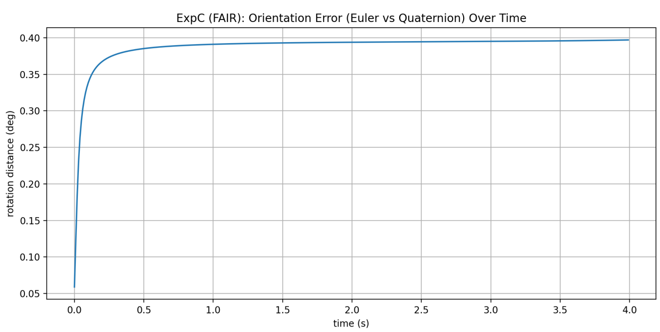

Fig. 5. Orientation error on $SO(3)$ between Euler-based and quaternion-based propagation under a pure yaw command near the gimbal-lock configuration.

Figure 5 illustrates the Euler-angle response under this input. Despite the absence of commanded roll motion, the Euler-based representation exhibits significant roll variation, indicating unintended yaw–roll coupling. This behavior arises because yaw and roll axes become aligned near $\theta \approx 90°$, causing a loss of independent rotational degrees of freedom.

In contrast, Fig. 6 shows the forward-axis deviation obtained from quaternion-based propagation. The forward vector rotates smoothly about the vertical axis, preserving the intended yaw-only motion without inducing spurious roll components.

This difference highlights a critical practical implication for drone navigation. In Euler-based systems, yaw commands near singular configurations can unintentionally introduce roll motion, potentially destabilizing the vehicle. Quaternion-based propagation, by maintaining a globally nonsingular orientation representation, preserves control intent and ensures that commanded motions correspond directly to physical behavior.

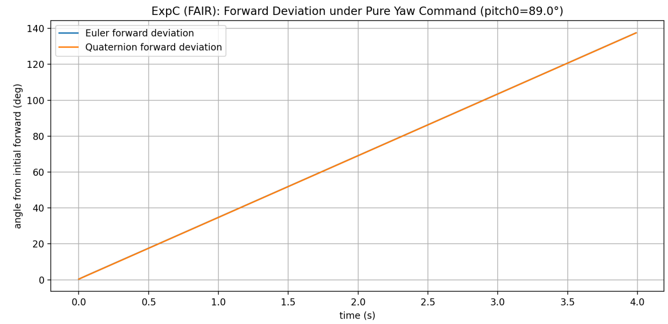

Fig. 6. Forward-axis deviation under a pure yaw command near the gimbal-lock configuration.

These experimental observations demonstrate that quaternions not only avoid the mathematical singularities of Euler angles but also eliminate control artifacts that can compromise stability and safety in real-world drone applications.

VII. Conclusion

Euler angles fail to provide a globally valid representation of three-dimensional orientation due to the presence of singular configurations. At the gimbal-lock condition, the Euler parameterization loses one degree of freedom, leading to non-unique representations, ill-conditioned kinematics, and unintended coupling between rotational axes. These failures were observed experimentally as instability in orientation propagation, divergence in rotation space, and distortion of control intent.

Importantly, gimbal lock was shown to be a mathematical artifact of the Euler-angle representation rather than a physical limitation of rotational motion. The underlying rigid-body dynamics remain well-defined; the observed failures arise solely from the choice of parameterization.

Quaternion-based orientation representations were shown to overcome these limitations by design. By providing a globally nonsingular parameterization of $SO(3)$, quaternions enable smooth and stable orientation propagation across all configurations, including those corresponding to Euler singularities. Experimental results confirmed that quaternion-based propagation preserves geometric consistency and control intent under conditions where Euler angles fail.

These findings highlight the practical importance of quaternion-based representations for aerial vehicles. In drone navigation and control systems, where robustness and stability are critical, the use of quaternions is essential to avoid singularity-induced artifacts and to ensure reliable orientation estimation and control.

APPENDIX

GitHub Repository

- Repository URL:
  Gimbal-Lock-Quaternion-Drone-Navigation
- Video:
  Presentation Video
- The repository contains the complete source code, experimental scripts, numerical outputs, and figures used to generate the results presented in this paper.
- All experiments can be reproduced by executing the provided scripts in the `src/` directory.

Code Structure Description

- `src/` contains the main source code used to implement orientation propagation, evaluation metrics, and experimental simulations.
- `src/expA_gimbal_lock.py` implements **Experiment A (Static Ambiguity)**, in which the pitch angle is fixed at $\theta = 90^\circ$ and multiple yaw–roll combinations are evaluated to demonstrate non-unique Euler parameterization.
- `src/expB_propagation_compare.py` implements **Experiment B (Dynamic Orientation Propagation)**, performing time-based integration for both Euler-angle-based and quaternion-based representations under identical angular velocity inputs.
- `src/expC_control_mixing.py` implements **Experiment C (Control Mixing)**, initializing the system near the gimbal-lock configuration ($\theta \approx 89^\circ$), applying a pure yaw angular velocity command, and measuring yaw–roll coupling and forward-axis deviation.
- Utility functions in `src/` provide:
  - conversion between Euler angles, quaternions, and rotation matrices,
  - Euler-rate mapping and quaternion kinematic propagation,
  - computation of orientation error on $SO(3)$,
  - computation of forward-vector deviation,
  - generation of plots and visualizations used in the paper.
- `output/` contains all experimental results and visualization files:
  - `output/expA_results.csv` and `output/expA_plot.png` store numerical and visual results for Experiment A.
  - `output/expB_results.csv`, `output/expB_angles_over_time.png`, `output/expB_euler_rates_over_time.png`, and `output/expB_orientation_error_over_time.png` store results for Experiment B.
  - `output/expC_results.csv`, `output/expC_forward_deviation.png`, `output/expC_orientation_error.png`, and `output/expC_euler_errors.png` store results for Experiment C.

Optional Mathematical Details

- Quaternion kinematic equation used for orientation propagation:
$$\dot{q} = \frac{1}{2}\Omega(\boldsymbol{\omega})q. \tag{28}$$
- Orientation error metric on $SO(3)$ used to compare Euler-based and quaternion-based propagation:
$$\theta = \cos^{-1}\left(\frac{\mathrm{trace}(R_1^T R_2) - 1}{2}\right). \tag{29}$$

ACKNOWLEDGMENT

I would like to express sincere gratitude to Dr. Ir. Rinaldi Munir, M.T., for his guidance and dedication in teaching the course IF2123 Aljabar Linier dan Geometri. His lectures throughout the semester provided the foundational understanding of linear algebra and geometry that made this work possible.

REFERENCES

[1] M. D. Shuster, "A survey of attitude representations," *Journal of the Astronautical Sciences*, vol. 41, no. 4, pp. 439–517, 1993.
[2] J. B. Kuipers, *Quaternions and Rotation Sequences: A Primer with Applications to Orbits, Aerospace, and Virtual Reality*. Princeton University Press, 1999.
[3] F. L. Markley and D. Mortari, "Quaternion attitude estimation using vector observations," *Journal of the Astronautical Sciences*, vol. 48, no. 2, pp. 359–380, 2003.
[4] H. Goldstein, C. Poole, and J. Safko, *Classical Mechanics*, 3rd ed. Addison-Wesley, 2002.
[5] J. Diebel, "Representing attitude: Euler angles, unit quaternions, and rotation vectors," Stanford University, Tech. Rep., 2006.
[6] D. Q. Huynh, "Metrics for 3d rotations: Comparison and analysis," *Journal of Mathematical Imaging and Vision*, vol. 35, no. 2, pp. 155–164, 2009.

DECLARATION OF ORIGINALITY

I hereby declare that the work presented in this paper is entirely my own. It is not a copy, translation, or adaptation of any other author's work, and it does not constitute plagiarism.

Bandung, December 23rd 2024

Agatha Tatianingseto – 13524008